PNAS RESEARCH ARTICLE | DEVELOPMENTAL BIOLOGY OPEN ACCESS

LST-1 is a bifunctional regulator that feeds back on Notch-dependent transcription to regulate *C. elegans* germline stem cells

Ahlan S. Ferdous[a,b], Tina R. Lynch[a,b], Stephany J. Costa Dos Santos[a], Deep H. Kapadia[a], Sarah L. Crittenden[a], and Judith Kimble[a,1]

Contributed by Judith Kimble; received June 13, 2023; accepted August 15, 2023; reviewed by Sarah J. Bray and Susan Strome

Notch signaling regulates stem cells across animal phylogeny. *C. elegans* Notch signaling activates transcription of two genes, *lst-1* and *sygl-1*, that encode potent regulators of germline stem cells. The LST-1 protein regulates stem cells in two distinct ways: It promotes self-renewal posttranscriptionally and also restricts self-renewal by a poorly understood mechanism. Its self-renewal promoting activity resides in its N-terminal region, while its self-renewal restricting activity resides in its C-terminal region and requires the Zn finger. Here, we report that LST-1 limits self-renewal by down-regulating Notch-dependent transcription. We detect LST-1 in the nucleus, in addition to its previously known cytoplasmic localization. LST-1 lowers nascent transcript levels at both *lst-1* and *sygl-1* loci but not at *let-858*, a Notch-independent locus. LST-1 also lowers levels of two key components of the Notch activation complex, the LAG-1 DNA binding protein and Notch intracellular domain (NICD). Genetically, an LST-1 Zn finger mutant increases Notch signaling strength in both gain- and loss-of-function GLP-1/Notch receptor mutants. Biochemically, LST-1 co-immunoprecipitates with LAG-1 from nematode extracts, suggesting a direct effect. LST-1 is thus a bifunctional regulator that coordinates posttranscriptional and transcriptional mechanisms in a single protein. This LST-1 bifunctionality relies on its bipartite protein architecture and is bolstered by generation of two LST-1 isoforms, one specialized for Notch downregulation. A conserved theme from worms to human is the coupling of PUF-mediated RNA repression together with Notch feedback in the same protein.

Notch signaling | smFISH | active transcription site | LAG-1 | NICD

Significance

Notch signaling controls stem cells across animal phylogeny and when unregulated can cause tumors. Nematode Notch activates transcription of two potent stem cell regulators, LST-1 and SYGL-1. Previous work established LST-1 and SYGL-1 as posttranscriptional regulators essential for self-renewal and oncogenic when overexpressed. Here, we report that LST-1 also feeds back on Notch-dependent transcription to limit self-renewal. LST-1 uses a C-terminal Zinc finger to weaken Notch strength and lower *lst-1* and *sygl-1* expression, whereas it uses N-terminal PUF-interacting motifs to repress RNAs. LST-1 emerges as a bifunctional regulator with intriguing parallels to fly and mammalian regulators. A conserved theme from worms to human is the coupling of PUF-mediated RNA repression together with Notch feedback in the same protein.

Stem cell self-renewal and differentiation must be balanced to generate functional tissues during development and to maintain them in adults. Signaling from a stem cell "niche" is responsible for self-renewal while escape from that signaling is required for differentiation (1). The strength of niche signaling is an important determinant of the balance between self-renewal and differentiation: Too much signaling can drive tumor formation and cancer (2, 3), while too little can lead to stem cell loss and tissue degeneration (4). Niche signaling strength must therefore be carefully regulated to ensure healthy tissues and avoid disease. Yet the complexity of most niches—often with multiple signaling sources and multiple signaling pathways (5–7)—presents a major challenge to teasing apart the in vivo mechanisms that regulate niche signaling strength.

C. elegans germline stem cells (GSCs) and their niche provide a uniquely tractable system to analyze in vivo regulatory mechanisms of self-renewal and differentiation (8, 9). That tractability is due in part to its unusual anatomical simplicity (Fig. 1*A*) and in part to the wealth of information available about its molecular regulation (Fig. 1*B*). Briefly, a single-celled niche maintains a pool of GSCs in the progenitor zone, a germline region that harbors stem cells distally and cells beginning differentiation proximally (Fig. 1*A*) (10). The niche employs Notch signaling to activate transcription of two genes, *lst-1* and *sygl-1* (Fig. 1*B*, *Left*) (11–14). The *lst-1* and *sygl-1* genes produce potent though functionally redundant stem cell regulators. The *lst-1* gene encodes two isoforms (Fig. 1*C*): The longer LST-1L isoform promotes stem cell self-renewal in the absence of *sygl-1*, while the shorter LST-1S isoform cannot (15). LST-1S is less studied and is poorly understood. Here, we use the term "LST-1" for simplicity, unless the two isoforms must be distinguished. Both LST-1 and SYGL-1 are posttranscriptional regulators (Fig. 1*B*, *Right*) (15, 16). Each binds to a PUF (for Pumilio and FBF) RNA-binding protein via PUF-interacting motifs that reside within a stretch of intrinsically disordered regions (Fig. 1*C*). The resultant LST-1/PUF and SYGL-1/PUF complexes repress RNAs and promote GSC self-renewal (15–17). Normally, PUF proteins are expressed throughout the progenitor zone, while their LST-1

Author contributions: A.S.F., T.R.L., and J.K. designed research; A.S.F., T.R.L., S.J.C.D.S., D.H.K., and S.L.C. performed research; A.S.F., T.R.L., S.J.C.D.S., S.L.C., and J.K. analyzed data; and A.S.F. and J.K. wrote the paper.

Reviewers: S.J.B., University of Cambridge; and S.S., University of California Santa Cruz.

The authors declare no competing interest.

[1]To whom correspondence may be addressed. Email: jekimble@wisc.edu.

This article contains supporting information online at https://www.pnas.org/lookup/suppl/doi:10.1073/pnas.2309964120/-/DCSupplemental.

Published September 20, 2023.

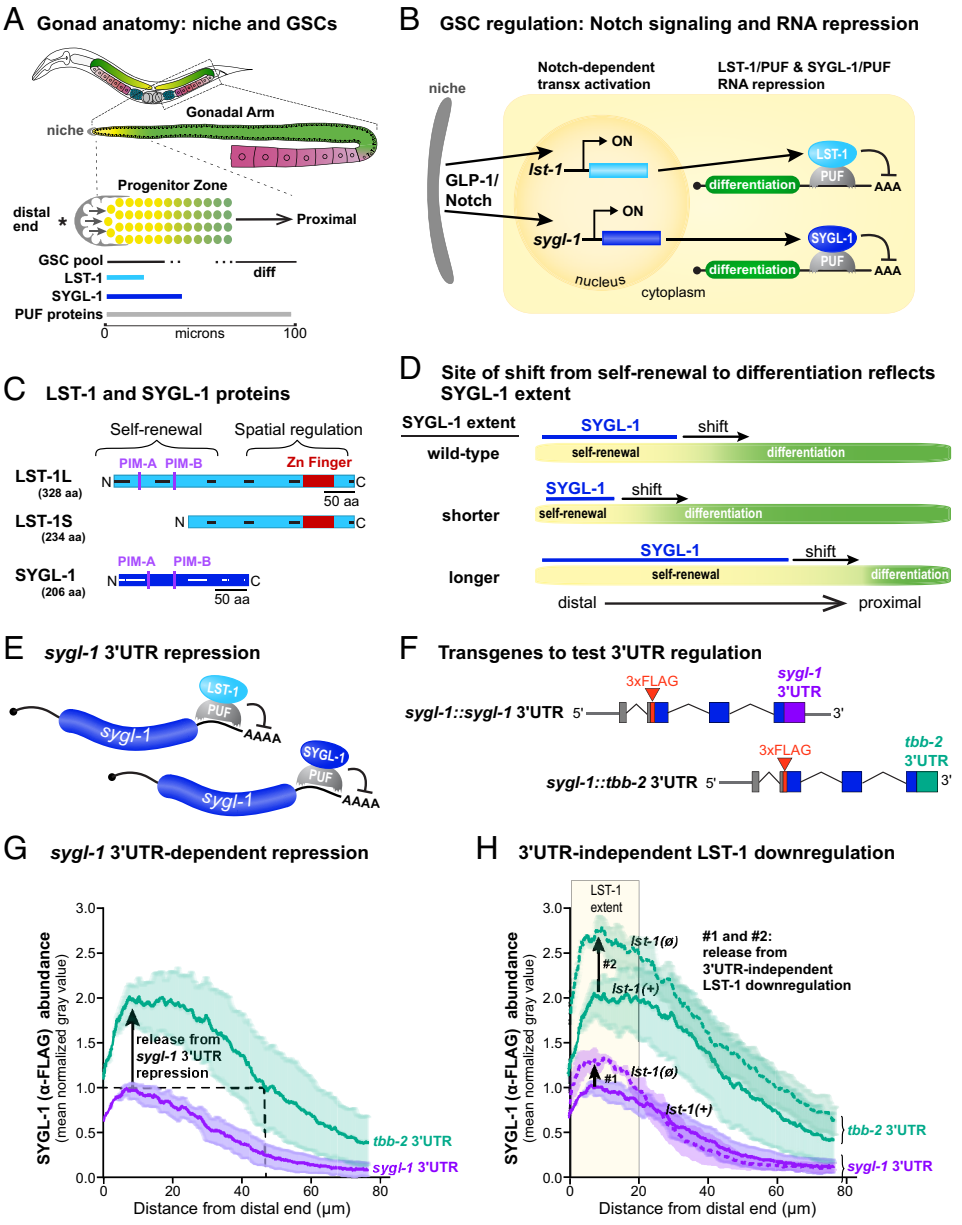

Fig. 1. Background and LST-1 down-regulates SYGL-1 independently of its 3′UTR. (*A*) Schematic of gonad anatomy. Above, animal with two gonadal arms. Middle, gonadal arm with stem cell niche (gray) and GSC pool (yellow) at the distal end and oocytes (rose) at the proximal end; differentiating germ cells are green before they make gametes. Below, progenitor zone. GSCs self-renew in the distal progenitor zone (yellow) and GSC daughters differentiate (green) as they progress proximally out of the niche. Extents of key GSC regulators and μm metric are shown below. (*B*) GSC molecular regulation, key features. The niche (gray) uses GLP-1/Notch signaling to activate transcription of *lst-1* and *sygl-1* genes in adjacent stem cell nucleus (yellow). *lst-1* and *sygl-1* produce LST-1 (blue) and SYGL-1 (dark blue) proteins, which partner with one of several PUF RNA-binding proteins (light gray) to repress mRNAs and promote self-renewal. (*C*) LST-1 and SYGL-1 proteins. LST-1 and SYGL-1 both possess two PUF-interacting motifs (PIM) (purple) and multiple regions of low complexity predicted to be intrinsically disordered (extents marked by short horizontal lines along protein axis; black for LST-1 and white for SYGL-1). LST-1L and LST-1S, the longer and shorter isoforms of LST-1, also have a single Nanos-like Zinc Finger (red). (*D*) Extent of SYGL-1 protein in the distal gonad correlates with germline shift from self-renewal to differentiation. Yellow, GSC pool; green, differentiation. (*E*) Model: LST-1/PUF and SYGL-1/PUF complexes bind *sygl-1* 3′UTR to repress *sygl*-1 RNA. 5′ cap, black circle; polyA tail, AAAA. (*F*) Transgenes used to test 3′UTR regulation. Above, *sygl-1* transgene bearing *sygl-1* 3′UTR; below, *sygl-1* transgene bearing *tbb-2* 3′UTR. All regions of both transgenes are derived from *sygl-1* locus with exception of *tbb-2* 3′UTR. Lines represent flanking regions and introns. Boxes are exons: 5′UTR, gray; coding region, dark blue; and 3′UTRs are either purple (*sygl-1*) or green (*tbb-2*). Modified from ref. 17. (*G* and *H*) SYGL-1^{FLAG} abundance determined by anti-FLAG staining (*y* axis) as a function of position in the progenitor zone (distance in μm from the distal end). (See Fig. 1*A* for metric). Data lines represent mean values of α-FLAG staining; shading shows SEM. Solid lines show SYGL-1 abundance in strains with wild-type *lst-1(+)*. Dotted lines show SYGL-1 abundance in *lst-1(ø)* strains that lack *lst-1*, Purple, data from *sygl-1* transgene with *sygl-1* 3′UTR; green, data from *sygl-1* transgene with *tbb2* 3′UTR. Both strains carry *sygl-1(ø)*, a deletion of the endogenous *sygl-1* gene. Background fluorescence from a no-tag control was subtracted to generate lines shown. Line from *sygl-1* 3′UTR strain was set to 1.0 at its peak and other lines were normalized to this value. Strain names and alleles are detailed in *SI Appendix*, Table S1. Lines in *G* are repeated in *H* for ease of comparison. (*G*) 3′UTR-dependent repression of *sygl-1* expression. Mean SYGL-1 abundance (*y* axis) as a function of distance from the distal end (*x* axis) from transgenes with *syg-1* 3′UTR (purple) or *tbb-2* 3′UTR (green), normalized to a no-tag control set at zero. Black dashed lines, SYGL-1 abundance from *tbb-2* 3′UTR transgene is higher than peak abundance from the *syg-1* 3′UTR transgene and extends much further along the gonadal axis. Upward arrow, 3′UTR-dependent change. Measurements were obtained from at least 25 gonads for each strain, assayed in two independent experiments. Total gonad numbers: *sygl-1* 3′UTR, n=28; *tbb-2* 3′UTR, n = 27; no-tag control, n = 25. (*H*) LST-1 downregulation is 3′UTR-independent. SYGL-1 abundance graphed as in *G* with same color coding and same *lst-1(+)* data. Expression is shown in *lst-1 (+)* (solid lines) and in *lst-1(ø)* strains (dotted lines). Upward arrows, 3′UTR-independent changes. Wild-type LST-1 is expressed in the four most distal germ cell rows (0 to 20 μm). LST-1 extent marked as pale yellow box. Gonad numbers for additional data with *lst-1(ø)*: *sygl-1* 3′UTR, n=28; *tbb-2* 3′UTR, n = 27. One-way ANOVA with Tukey's post hoc test was used to test the significance of differences for each of the following compared to *lst-1(+)lst-1 (ø)* $P < 0.01$; *lst-1 (+) tbb-2 3′UTR*, $P < 0.001$ and *lst-1(ø) tbb-2 3′UTR*, $P < 0.001$. There was also a statistically significant difference between *lst-1 (+) tbb-2 3′UTR* and *lst-1(ø) tbb-2 3′UTR*: P-< 0.01.

and SYGL-1 partners are restricted to the distal progenitor zone (Fig. 1*A*). Both LST-1L and LST-1S are expressed there, but LST-1L is more abundant than LST-1S while LST-1S extends a bit more proximally than LST-1L (15). Niche signaling therefore drives GSC self-renewal by triggering the localized assembly of LST-1/PUF and SYGL-1/PUF complexes in the distal progenitor zone.

Germ cells self-renew when they possess LST-1/PUF or SYGL-1/PUF, but they differentiate when LST-1 and SYGL-1 are lost (11, 17). The spatial extents of LST-1 and SYGL-1 along the axis of the progenitor zone therefore determine where germ cells self-renew and where they transition to differentiation. Driving ubiquitous expression of either LST-1 or SYGL-1 creates a germline tumor with self-renewing germ cells throughout the gonad (17), and removal of both LST-1 and SYGL-1 eliminates stem cells (11). However, in a normal gonad, self-renewal and differentiation are balanced along the progenitor zone axis to achieve a functional germline tissue (Fig. 1*A*). The strength of Notch signaling is a major determinant of LST-1 and SYGL-1 spatial extents (14, 18), and the *sygl-1* 3′UTR is another (17). Because SYGL-1 extends more proximally than LST-1 in wild-type gonads (Fig. 1*A*), the SYGL-1 extent normally determines where

GSCs self-renew or differentiate (Fig. 1*D*, top diagram). When the *sygl-1* 3'UTR is replaced with a tubulin *tbb-2* 3'UTR, SYGL-1 extent expands and the balance between self-renewal and differentiation shifts proximally, enlarging the GSC pool (Fig. 1*D*, middle diagram) (17); by contrast, when the *sygl-1* promoter is weakened by mutating Notch-dependent promoter elements, the SYGL-1 extent shrinks and the balance is shifted distally to shrink the GSC pool (Fig. 1*D*, bottom diagram) (18). These manipulations demonstrate unequivocally that the extent of SYGL-1 is a critical determinant of the balance between self-renewal and differentiation and GSC pool size.

This current study springs from two unexpected findings. First, a control experiment for analyses of *sygl-1* promoter mutants found that LST-1 lowers SYGL-1 protein abundance (18). Second, a structure–function analysis of LST-1 revealed negative autoregulation (15). Here, we investigate the mechanism underlying these findings. We first exclude a posttranscriptional mechanism and then show that LST-1 is nuclear, feeds back negatively on Notch-dependent transcription, and likely works directly to dampen strength of the Notch transcriptional activation complex. With its well-established role in posttranscriptional regulation and this previously unknown role in Notch-dependent transcription, LST-1 emerges as a bifunctional regulator of stem cells—promoting their self-renewal posttranscriptionally and limiting self-renewal at a transcriptional level.

Results

LST-1 Down-Regulates SYGL-1 Independently of the *sygl-1* 3'UTR. We first explored the simple idea that LST-1 might down-regulate LST-1 and SYGL-1 expression posttranscriptionally (Fig. 1*E*). We focused on *sygl-1* because reagents were available. Using transgenic animals carrying FLAG-tagged *sygl-1* transgenes with either a *sygl-1* or *tbb-2* 3'UTR (Fig. 1*F* and *SI Appendix*, Fig. S1*A*) (17), we first confirmed that the *sygl-1* 3'UTR is repressive (Fig. 1*G* and *SI Appendix*, Fig. S1*B*). The *tbb-2* 3'UTR-bearing transgene made about twice as much SYGL-1 as the *sygl-1* 3'UTR-bearing transgene when measured at peak abundance (Fig. 1*G*, upward arrow), and it expanded the extent of high SYGL-1 along the gonadal axis (Fig. 1*G*, dotted line). If LST-1 downregulation of SYGL-1 were exerted solely through the *sygl-1* 3'UTR, LST-1 removal should not further change SYGL-1 abundance. However, genetic removal of LST-1 led to an additional increase in SYGL-1 abundance, regardless of its 3'UTR (Fig. 1*H*, upward arrows #1 and #2). The increases were limited to the distal-most germ cells (Fig. 1*H*), where LST-1 is expressed (pale yellow box) (15, 17). Although the magnitudes of increases were small and differ from each other, the key point is that the increases exist and are significant. We conclude that LST-1 down-regulates SYGL-1 expression by a mechanism independent of 3'UTRs in addition to its well-established 3'UTR dependent role.

LST-1 Protein can be Detected in Germline Nuclei. What is the 3'UTR-independent mechanism? A genome-wide two-hybrid screen had found that LST-1 interacts physically with several transcription factors in yeast (19). We therefore wondered whether some fraction of LST-1 might be nuclear and regulate transcription in addition to its cytoplasmic posttranscriptional role. To visualize LST-1, we used a 3xV5 epitope-tagged allele of endogenous *lst-1*, which tags both isoforms and has normal biological activity (15). We costained dissected gonads with α-V5 antibodies to visualize LST-1^{V5}, α-LMN-1 antibodies to outline the nuclear envelope and DAPI to see DNA (Fig. 2 *A* and *B*). Most LST-1^{V5} localized to perinuclear and cytoplasmic granules (Fig. 2*A*), as previously reported (15). However, we also detected LST-1^{V5} inside nuclei, when imaged with a laser scanning confocal microscope and examined in single z-slices at high resolution. Nuclear LST-1^{V5} was present in the distal-most GSCs near the niche (Fig. 2*B*, left images), but not in more proximal germ cells (Fig. 2*B*, right images). We then quantified nuclear LST-1^{V5} as a function of position along the progenitor zone axis (Fig. 2*C*), comparing the V5 signal to that in a wild-type control with no V5. LST-1^{V5} was easily seen in nuclei 1 to 3 germ cell diameters (gcd) from the distal end, but signal decreased to control levels by five gcd. Finding LST-1^{V5} in the nucleus inspired us to ask whether it regulates transcription.

LST-1 Regulates *sygl-1* Transcription. To assess LST-1 effects on transcription, we dissected gonads from adults and scored nascent transcripts at individual active transcription sites (ATS) in nuclei. We used single-molecule fluorescence in situ hybridization (smFISH) to visualize ATS (Fig. 3*A*), with probes specific to introns of the Notch-dependent *sygl-1* locus and the Notch-independent *let-858* locus (Fig. 3*B*). MATLAB image analysis software was used for ATS detection and quantification, as done previously (14).

We first quantitated the total number of *sygl-1* ATS per germline in wild-type *lst-1(+)* and null *lst-1(ø)* gonads. The bulk number of *sygl-1* ATS was ~twofold higher in *lst-1(ø)* than *lst-1(+)* germlines (Fig. 3*C*). We next scored percentage of cells possessing any *sygl-1* ATS, a measure of transcriptional probability (14), as a function of position along the gonad axis (Fig. 3*D*). The *sygl-1* transcriptional probability was also higher in *lst-1(ø)* than *lst-1(+)* germlines and that increase was greatest in the distal-most germ cells where LST-1 is normally expressed (Fig. 3*D*, pale yellow bar). Wild-type LST-1 therefore lowers the level of *sygl-1* transcription in GSCs.

We next asked whether LST-1 affects transcription of a Notch-independent gene. The *let-858* gene is not controlled by Notch signaling and is expressed throughout the germline (14). In contrast to *sygl-1* ATS, the total number of *let-858* ATS was the same in *lst-1(+)* and *lst-1(ø)* germ cells (Fig. 3*E*), and the *let-858* transcriptional probability was similarly unchanged (Fig. 3*F*). The LST-1 lowering of *sygl-1* transcription is therefore not general and may target Notch-dependent transcription specifically.

The LST-1 C-Terminal Region Is Required to Regulate *sygl-1* Transcription. To identify the region of the LST-1 protein responsible for down-regulating *sygl-1* transcription, we took advantage of a set of previously characterized LST-1 variants, all except *lst-1(ø)* with a C-terminal 3xV5 tag (Fig. 4*A*) (15). Two variants lack either the N- or C-terminal regions. The C-terminal deletion (CΔ) leaves LST-1 with its N-terminal 211 amino acids (out of 328); this variant retains its PUF interacting motifs (PIMs) and removes its Zinc finger (Fig. 4*A*). NΔ is not a physical deletion, but instead is a stop mutation engineered at the LST-1L start codon. This mutation effectively removes LST-1L and retains LST-1S as the only isoform (15). Assayed without SYGL-1 to avoid redundancy, the truncated CΔ variant was sufficient to maintain GSCs, but NΔ was not (15).

We compared ATS generation from *sygl-1* and *let-858* loci in four different strains. Transcription from *sygl-1* increased relative to wild type in both *lst-1(CΔ)* and *lst-1(ø)* mutants, scored either as the total number of ATS (Fig. 4*B*) or transcriptional probability (*SI Appendix*, Fig. S3*A*), whereas *sygl-1* transcription was unchanged in *lst-1(*NΔ) mutants (Fig. 4*B* and *SI Appendix*, Fig. S3*A*). By contrast, *let-858* transcription was the same in all variants (Fig. 4*C* and *SI Appendix*, Fig. S3*B*). We conclude that

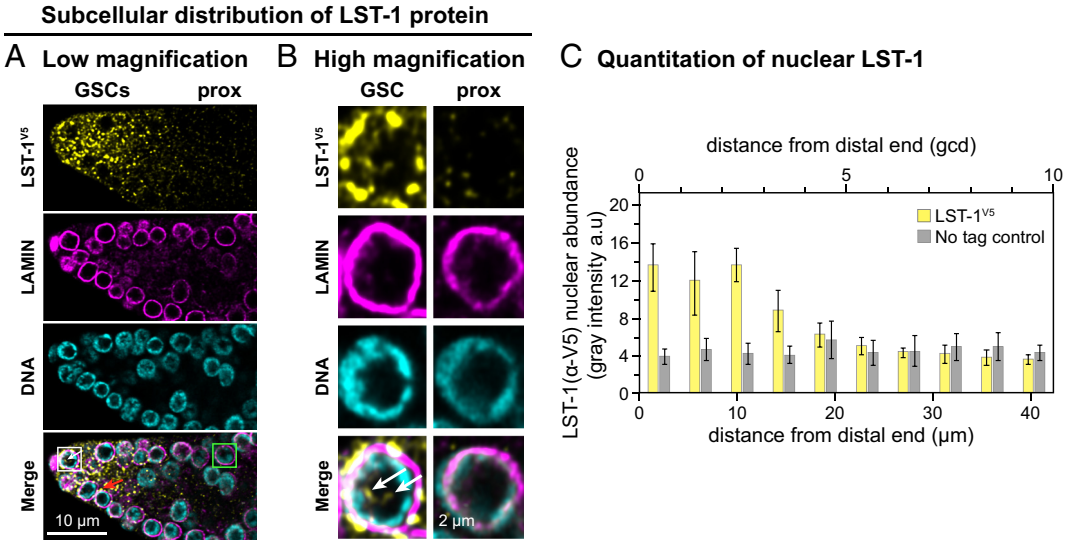

Fig. 2. LST-1 protein can be detected in GSC nuclei. (*A*) Low magnification of LST-1^{V5} staining in the distal gonad. Representative deconvolved single confocal *z*-slices from the middle plane of the distal region of an extruded gonad. Row-1, α-V5 detects LST-1^{V5} (yellow); row-2, α-LMN-1 detects LAMIN-1 in the inner nuclear envelope (magenta); row-3, DAPI highlights DNA in nuclei (cyan); row-4, merged images show LST-1^{V5} in the cytoplasm (red arrowhead) and nucleus (white arrow). White box, GSC nucleus magnified in Fig. 2*B*; green box, more proximal (prox) nucleus magnified in Fig. 2*B*. (*B*) High magnification of boxed regions in (*A*). Arrows mark nuclear LST-1. (*C*) Abundance of nuclear LST-1^{V5} as a function of position in the progenitor zone, measured in germ cell diameter (gcd) from the distal end (above) and converted to distance in µm from the distal end (below) by a conversion factor of 4.4 gcd/ µm. Measurements combine three independent replicates. LST-1^{V5}, n = 33 gonads; No tag control (N2), n = 30 gonads.

the activity responsible for regulating *sygl-1* transcription resides in the LST-1 C-terminal region.

LST-1 Zn Finger Is Required to Regulate Notch-Dependent Transcription. A single predicted CCHC Zn finger (ZnF) resides within the C-terminal region (Fig. 4*A*). An *lst-1(ZnF)* mutant destroys this Zn finger by substituting serines for two structurally critical cysteines (C260S and C263S) (15). The LST-1(ZnF)^{V5} mutant protein retains its ability to maintain stem cells but loses its ability to autoregulate (15). We therefore surmised that the Zn finger might be critical for LST-1 transcriptional regulation.

To test this idea, we first assessed *sygl-1* ATS in *lst-1(+)* and *lst-1(ZnF)* variant germlines. For this analysis, we used probe sets to both *sygl-1* exons and introns (Fig. 4*D*) and detected *sygl-1* ATS from the overlap of their signals with MATLAB, as done previously (14, 18, 20). Both total number of *sygl-1* ATS (Fig. 4*F*) and *sygl-1* transcriptional probabilities (Fig. 4*G*) increased significantly in the LST-1 Zn finger mutant. Moreover, the increase was restricted to the region where LST-1 protein is expressed (Fig. 4*G*, pale yellow box). The LST-1 Zn finger is thus required to lower *sygl-1* transcription.

We next asked whether autoregulation of *lst-1* expression also relies on a transcriptional mechanism. The original study identifying this autoregulation did not score *lst-1* ATS but instead quantified *lst-1* cytoplasmic mRNAs (15); this approach was taken because detection of *lst-1* ATS was challenging using MATLAB (14). In those previous studies, *lst-1* ATS needed to be confirmed manually due to low signal to noise ratio. Because Imaris image analysis software filters out false positive results more efficiently, we turned to Imaris to detect and quantitate *lst-1* ATS in this paper (see Methods). For this analysis, we used probe sets to both *lst-1* exons and introns (Fig. 4*E*), as explained for *sygl-1*. To validate our use of Imaris, we compared it to MATLAB for detection of *sygl-1* ATS and obtained comparable results (*SI Appendix*, Fig. S3). We also included two controls to validate positive *lst-1* signals, *lst-1(ø)* and no probes (Fig. 4*H*). The *lst-1* ATS were significantly increased in *lst-1(ZnF)* mutants, both total number (Fig. 4*H*) and transcriptional probabilities (Fig. 4*I*). As with *sygl-1*, the *lst-1* ATS increase was restricted to the region where LST-1 is expressed (Fig. 4*I*, pale yellow box). More *sygl-1* ATS were detected than *lst-1* ATS in wild type, as reported previously Lee et al. (14). However, ATS number roughly doubled in the *lst-1(ZnF)* variant for both genes. We conclude that the LST-1 Zn finger is required to lower both *lst-1* and *sygl-1* transcription, consistent with an effect on Notch-dependent transcription.

We also asked whether the LST-1 PIMs affect either *sygl-1* or *lst-1* transcription. PIMs were already established as essential for posttranscriptional regulation (15, 16), but a transcriptional role had not been tested. We found that both *sygl-1* ATS and *lst-1* ATS were comparable in *lst-1(+)* and *lst-1(PIM)* mutants (*SI Appendix*, Fig. S3 *C–F*). Therefore, the *lst-1(PIM)* mutant retains its ability to lower Notch-dependent transcription. The LST-1 PIMs are thus specialized for posttranscriptional regulation.

LST-1 Lowering of Notch-Dependent Transcription May Be Direct. Finding LST-1^{V5} in the nucleus (Fig. 2) suggested that the LST-1 might lower Notch-dependent transcription via effects on the Notch-dependent transcription activation complex. Fig. 5*A* summarizes key players of that complex in their nematode context. Notch ligand binds to the GLP-1/Notch receptor at the cell surface, induces receptor cleavage, and frees the Notch intracellular domain (NICD) to enter the nucleus. Once in the nucleus, the NICD assembles into the activation complex to drive transcription of Notch-dependent targets genes, such as *sygl-1* (21). Central to the complex is the conserved CSL (CBF-1/Su(H)/LAG-1) DNA binding protein, called LAG-1 in nematodes (22). The aforementioned genome-wide two-hybrid screen identified LAG-1 as interacting with LST-1 in yeast (19), so we set out to test the possibility of a physical association between LST-1 and LAG-1 in nematodes.

To test for co-immunoprecipitation of LST-1 and LAG-1, we inserted 3X FLAG at the LAG-1 C terminus in the endogenous *lag-1* gene. We then made strains carrying *lag-1*^{FLAG}, *glp-1(gf ts)*

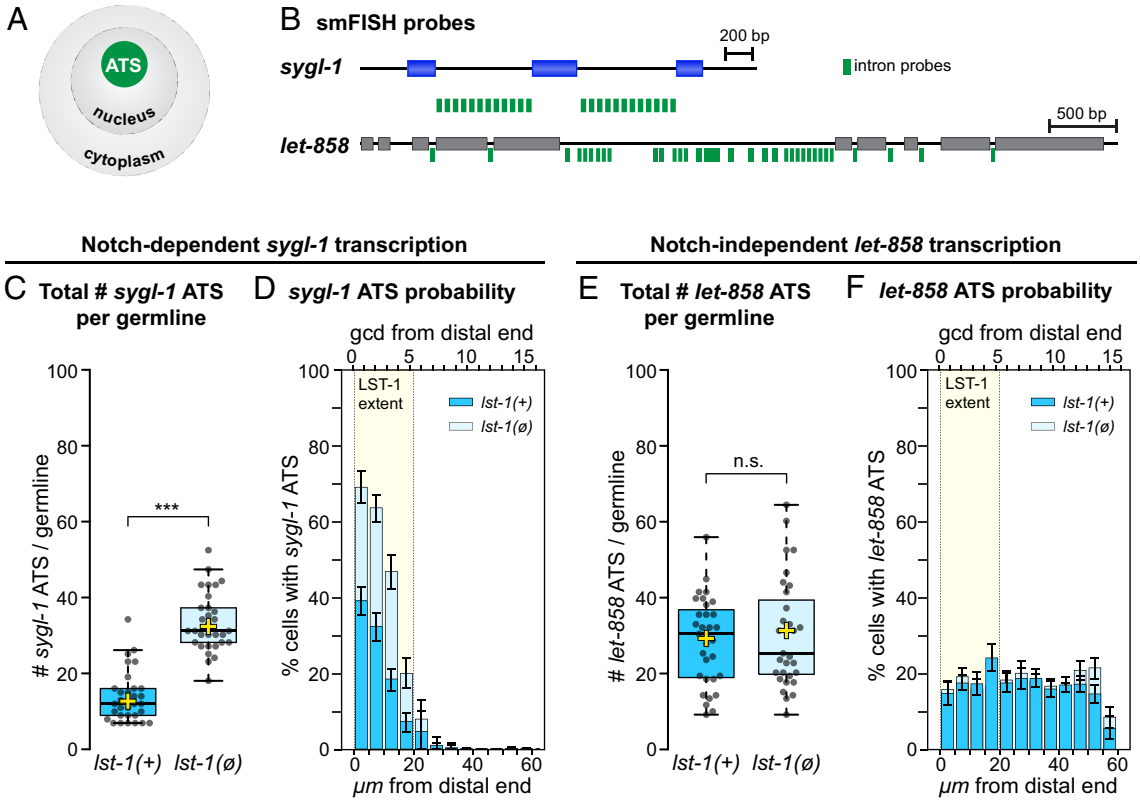

Fig. 3. LST-1 down-regulates Notch-dependent transcription. (*A*) Schematic of active transcription site (ATS) detection. smFISH probes hybridize to nascent transcripts at chromosomal sites being actively transcribed. (*B*) *sygl-1* and *let-858* genes showing positions of smFISH probes used to detect their nascent transcripts. Boxes are exons; lines are introns and flanking regions. See *SI Appendix*, Table S3 for probe sequences. (*C–F*) *sygl-1* ATS and *let-858* ATS were scored in bulk or by position using MATLAB to score signals from intron probes to each gene. For *let-858,* exon probes were not available. *lst-1(+)* refers to the wild-type gene; *lst-1(ø)* refers to a null allele. See *SI Appendix*, Table S1 for strain and allele numbers. (*C* and *E*) Boxplots showing the total number of ATS per germline, scored in *lst-1(+)* wild-type gonads (left, blue) and *lst-1(ø)* null mutant gonads (right, pale blue). ATS were scored at a V5-tagged endogenous *sygl-1* locus, which we call *sygl-1* for simplicity. Each dot represents total *sygl-1* ATS from a single germline. Boxes, 25 to 75% quantile; middle line, median; yellow plus, mean; whiskers, minimum and maximum values. Asterisks indicate statistically significant differences (pair-wised Student's *t*.Test): *P-values*, ** < 0.001, ***< 0.0001. n.s., not significant ($P > 0.05$). (*D* and *F*) Bar graphs showing the percentage of cells with any ATS (*y* axis) as a function of gonadal position (*x* axis), scored in wild-type *lst-1(+)* gonads (blue) and *lst-1(ø)* null mutant gonads (pale blue bars). Positions are indicated as distance from the distal end measured in µm at the bottom and in germ cell diameters (gcd) at the top. Error bars represent SEM.

and either *lst-1(+)*^{V5} or *lst-1(ZnF)* ^{V5}. The *glp-1(gf ts)* mutant was included to facilitate LST-1 IPs, as done previously (16). At permissive temperature (15 °C), most *glp-1(gf ts)* mutants have normal fertile germlines, but at restrictive temperature (25 °C), excess Notch signaling drives formation of germline tumors (23). As a direct Notch target, LST-1^{V5} is expressed throughout the *glp-1(gf ts)* tumors so its levels are higher in bulk lysates, though not in individual cells (16). In the strains made for the current study, most *glp-1(gf ts)* strains made normal germlines at 15 °C (<2% with tumors) as expected, (Fig. 5 *B*, *i*), but there was one notable exception. Nearly half the *glp-1(gf ts)* animals carrying the *lst-1(ZnF)* mutant had germline tumors at 15 °C (Fig. 5 *B*, *i*, fourth line). The *lst-1(ZnF)* mutant thus enhances the *glp-1(gf ts)* tumor defect. To complement this result, we tested *glp-1(lf ts),* a weak loss of function receptor mutant (Fig. 5 *B*, *ii*) (10). Whereas *glp-1(lf ts)* mutants were all sterile at the restrictive temperature of 25°, most *lst-1(ZnF); glp-1(lf ts)* double mutants were fertile at 25° (Fig. 5 *B*, *ii*, third line). The *lst-1(ZnF)* mutant thus suppresses *glp-1(lf ts)* sterility. These two results—enhancing gain-of-function and suppressing loss-of-function mutants of the GLP-1/Notch receptor—show that disruption of the LST-1 Zinc finger increases Notch signaling strength.

Once strains were built and characterized, we tested for co-immunoprecipitation of LST-1 and LAG-1. We pulled down LAG-1^{FLAG} from nematode extracts and detected co-immunoprecipitating proteins on western blots (Fig. 5*C*). The two wild-type LST-1 isoforms, LST-1L^{V5} and LST-1S^{V5} co-immunoprecipitated robustly (Fig. 5*C*, middle lane), showing that both physically associate with LAG-1. We predicted that LST-1 Zinc finger mutant proteins would not coIP but got an unexpected result. The long LST-1L(ZnF)^{V5} isoform co-IP'd well with LAG-1, but the short LST-1S(ZnF)^{V5} isoform did not (Fig. 5*C*, right lane). This result was reproducible (*SI Appendix*, Fig. S4*B*). One explanation might have been that the two isoforms differ in nuclear localization. To address this possibility, we imaged the isoforms individually. A 3xFLAG tag at the N terminus of LST-1L is specific to the long isoform, because LST-1S lacks this N-terminal region. A C-terminal V5 tag of LST-1(NΔ) is specific to the short isoform because no LST-1L is made in this variant (15). We stained gonads for the two individual isoforms and costained for lamin and DNA, as in Fig. 2. Both LST-1L^{FLAG} and LST-1S^{V5} isoforms were found in nuclei (Fig. 5*D*). Another explanation for the isoform-specific pull down might be that the long isoform LST-1L(ZnF)^{V5} mutant protein retains its association with LAG-1, either via other parts of the LST-1L protein or other parts of the Notch transcription complex. Regardless, we conclude that LAG-1 physically associates with both LST-1L^{V5} and LST-1S^{V5}.

LST-1 Lowers Abundance of Two Key Components of the Notch Activation Complex. To learn more about how LST-1 and its Zn finger lower Notch signaling strength, we explored effects

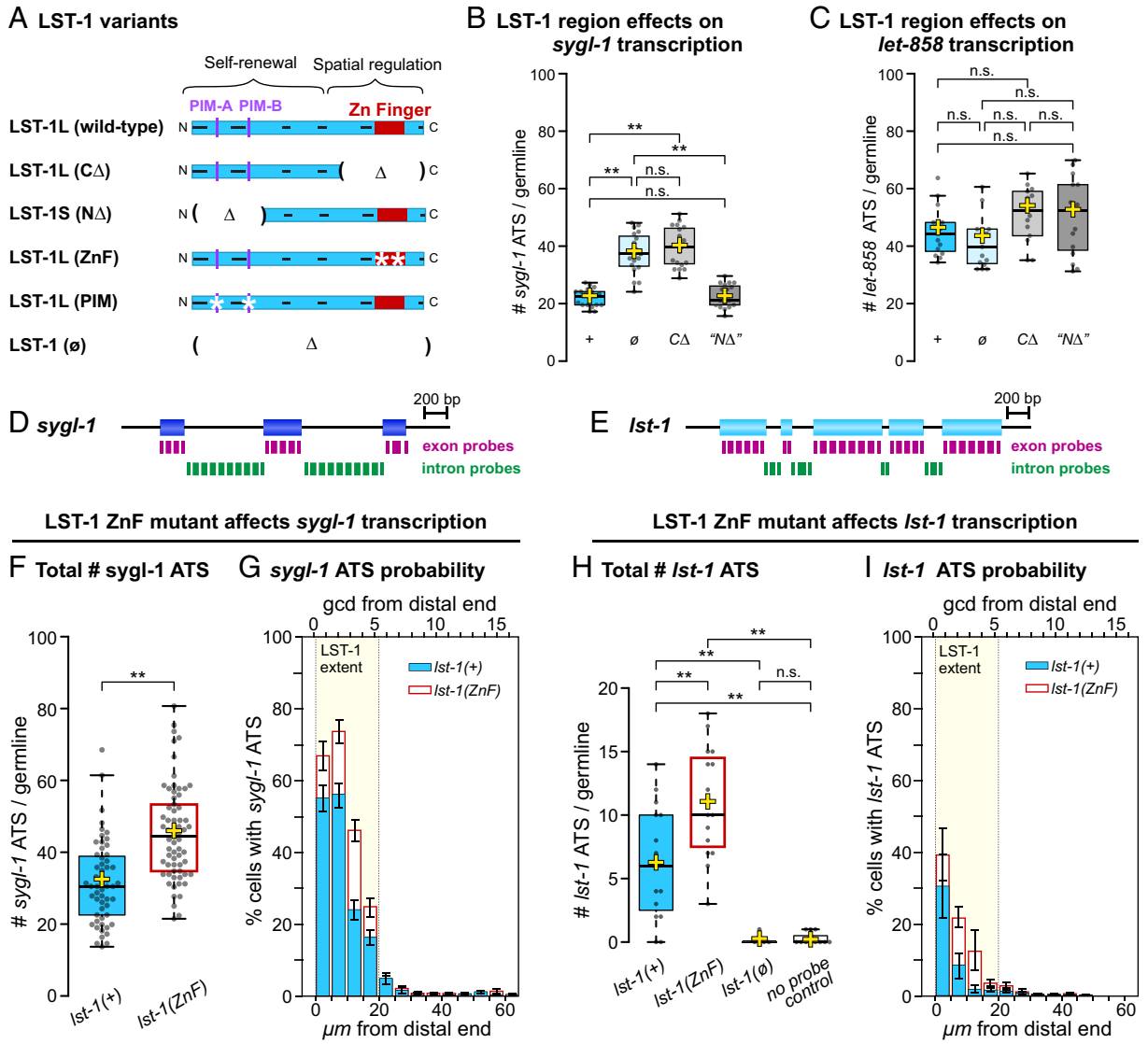

Fig. 4. LST-1 Zinc finger is required to lower *sygl-1* and *lst-1* transcription. (*A*) LST-1 protein variants used in this study (features as in Fig. 1*C*) (15). LST-1S not shown for simplicity. All except *lst-1(ø)* harbor a C-terminal 3× V5 tag (inverted triangle). LST-1 (CΔ) deletes the C-terminal region (amino acids 211 to 328); LST-1 (NΔ) carries a nonsense mutation early in LST-1L and makes only LST-1S, which lacks the N-terminal region unique to LST-1L (amino acids 1 to 94); LST-1 (ZnF) substitutes two key cysteines with serines (C260S and C263S, asterisks); LST-1(PIM), substitutes key amino acids for alanines in both PIM-A and PIM-B (L35A, K80A and L83A, asterisks) and abolishes LST-1 interactions with PUF proteins in both yeast and nematodes (15, 16). (*B–I*) Boxplot and bar graph conventions as described in the Fig. 3 legend. (*B* and *C*) Boxplots showing the total number of *sygl-1* ATS (*B*) or *let-858* ATS (*C*) in variants lacking either N-terminal or C-terminal LST-1 regions as shown in Fig. 4*A*. smFISH was done using intron probe sets as in Fig. 3*B* MATLAB quantitation as in Fig. 3 *C–F*. (*B*, *C*, and *H*) Asterisks indicate statistically significant differences (one-way ANOVA with Tukey's post hoc test): *P-values*, ** < 0.001, n.s., not significant (*P* > 0.05). (*D* and *E*) *sygl-1* ATS (*D*) and *lst-1* ATS (*E*) were scored as overlapping signals from exon and intron probes using MATLAB (*sygl-1)* or Imaris (*lst-1)* quantitation. Both exon and intron probes were available (in contrast to the case for *let-838).* (*F–I*) LST-1 Zn finger tested for effects on *sygl-1* ATS (*F* and *G*) and *lst-1* ATS (H-I). *lst-1(+)* gonads, blue; mutant *lst-1(ZnF)* gonads, red outline. (*F*) Total number *sygl-1* ATS per germline. Asterisks indicate statistically significant differences (pair-wised Student's *t*.Test): *P-values*, ** < 0.001, ***< 0.0001. n.s., not significant (*P* > 0.05). (*G*) Percentage cells with any *sygl-1* ATS (*y* axis) as a function of gonadal position (*x* axis). (*H*) Total number *lst-1* ATS per germline. (*I*) Percentage cells with any *lst-1* ATS (*y* axis) as a function of gonadal position (*x* axis).

on abundance of two key components of the Notch activation complex, LAG-1 and the GLP-1/Notch NICD (Fig. 5*A*). We first imaged LAG-1^{FLAG} (*SI Appendix*, Fig. S4*C*). LAG-1^{FLAG} was easily detectable in the distal gonads of *lst-1(+) and lst-1(PIM)*, and appeared to increase in *lst-1(ø)* and *lst-1(ZnF)*. Quantitation confirmed that LAG-1 was indeed more abundant in *lst-1(ø)* and *lst-1(ZnF)* than in *lst-1(+)* and *lst-1(PIM)* germlines (Fig. 5*E*). The increase was small (~1.3 fold at its peak) but significant. Therefore, wild-type LST-1 lowers LAG-1 abundance and its Zinc finger is critical for this effect.

We next imaged GLP-1/Notch NICD in the same *lst-1* variant gonads. To visualize the NICD, we used a GLP-1 receptor fused to Halo-tag at its C terminus, which generates a Halo-tagged receptor in membranes and upon cleavage, a Halo-tagged NICD in nuclei (24). We costained distal gonads with the Halotag ®TMR fluorescent ligand to detect the NICD, anti-lamin antibodies to outline the nuclear envelope, and DAPI to see DNA. Signal in the nucleus was low but detectable (*SI Appendix*, Fig. S4*D*). For quantitation, we chose a mid z-plane that included a visible distal tip cell to measure NICD abundance in nuclei of each germ cell row along the axis of the distal gonad. NICD levels were significantly higher in *lst-1(ø)* and *lst-1(ZnF)* mutants than in *lst-1(+)* or *lst-1(PIM)* mutants (Fig. 5*F*). The NICD increase was most pronounced in the germ cells where LST-1 is expressed (1 to 5 gcd) (Fig. 5*F*, pale yellow bar), and at its peak, was ~2.5-fold higher in *lst-1(ø) and lst-1(ZnF)* mutants than in *lst-1(+)* or *lst-1(PIM)* mutants. We

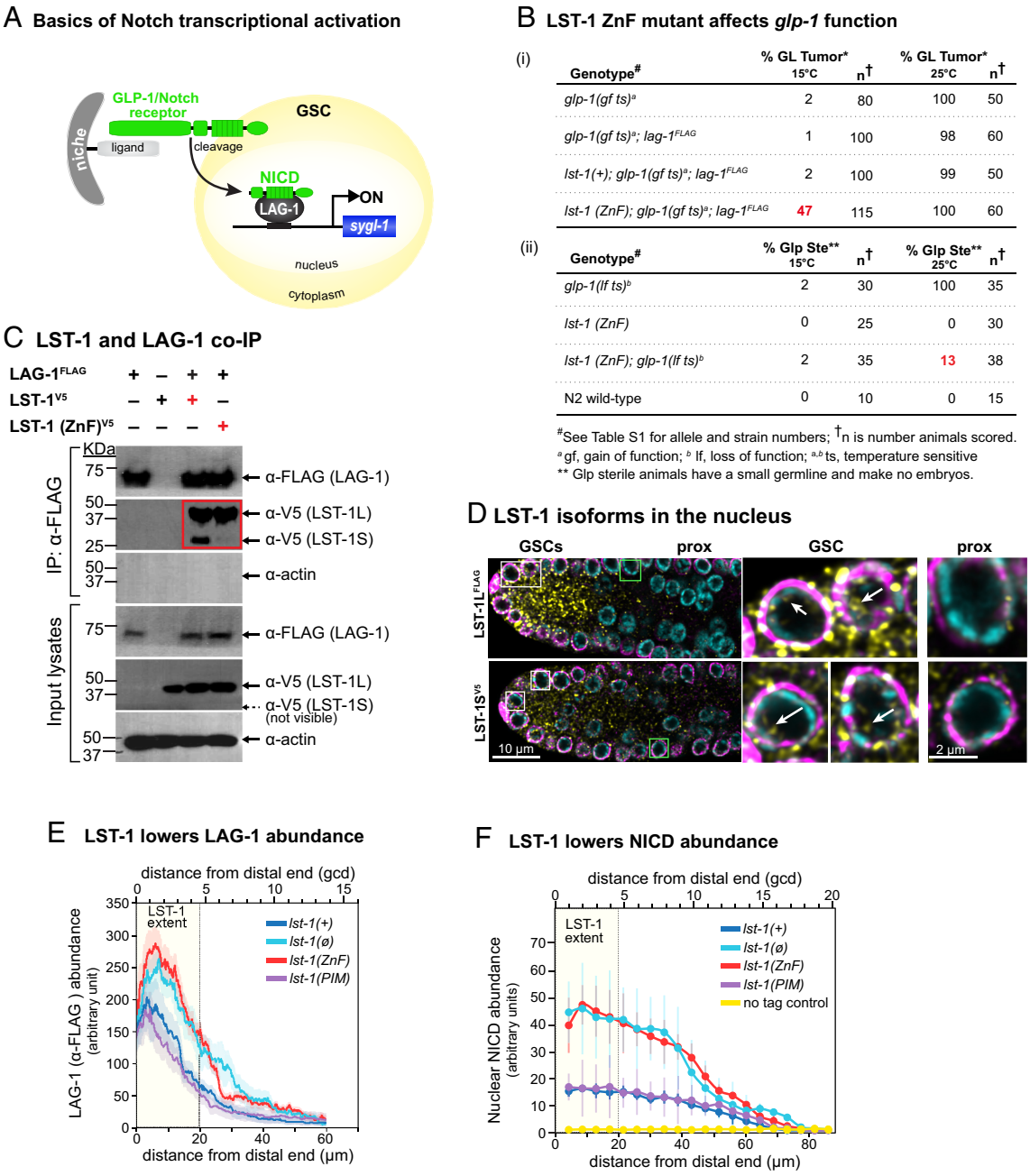

B LST-1 ZnF mutant affects *glp-1* function

(i)

Genotype#	% GL Tumor* 15°C	n†	% GL Tumor* 25°C	n†
glp-1(gf ts)[a]	2	80	100	50
glp-1(gf ts)[a]*; lag-1*[FLAG]	1	100	98	60
lst-1(+); glp-1(gf ts)[a]*; lag-1*[FLAG]	2	100	99	50
lst-1 (ZnF); glp-1(gf ts)[a]*; lag-1*[FLAG]	47	115	100	60

(ii)

Genotype#	% Glp Ste** 15°C	n†	% Glp Ste** 25°C	n†
glp-1(lf ts)[b]	2	30	100	35
lst-1 (ZnF)	0	25	0	30
lst-1 (ZnF); glp-1(lf ts)[b]	2	35	13	38
N2 wild-type	0	10	0	15

#See Table S1 for allele and strain numbers; †n is number animals scored.
[a] gf, gain of function; [b] lf, loss of function; [a,b] ts, temperature sensitive
** Glp sterile animals have a small germline and make no embryos.

Fig. 5. (*A*) LST-1 regulation of Notch-dependent transcription is likely direct. Schematic of Notch-dependent transcriptional activation of *sygl-1* target gene, showing two key components of the activation complex, the LAG-1 DNA-binding protein (dark gray) and Notch intracellular domain NICD (green). Niche, gray; Notch ligand, light gray; GSC, yellow; GLP-1/Notch receptor, green. (*B*) Genetic evidence that mutant in LST-1 Zn finger increases Notch signaling strength. (*i*) The normally low tumor penetrance of *glp-1(gf ts)* at permissive temperature (15 °C) is enhanced by *lst-1* Zinc finger mutant (red). (*ii*) The normally high sterility penetrance of *glp-1(lf ts)* at restrictive temperature (25 °C) is suppressed by *lst-1* Zinc finger mutant (red). (*C*) LST-1 and LAG-1 co-immunoprecipitate from nematodes in a ZnF-dependent manner (red box). Co-immunoprecipitations were done with lysates made from *glp-1 (ts gf)* mutants grown at 25 °C. Shown are western blots of input lysates and IP-eluted samples after formaldehyde cross-linking of whole worms and LAG-1^{FLAG} immunoprecipitation, probed with antibodies to detect LAG-1^{FLAG}, LST-1^{V5}, LST-1(ZnF)^{V5} and the actin loading control. 2% of input lysates and 20% of IP-eluted samples were loaded. Exposure times were different for input and IP lanes, so band intensities are not comparable. The coIPs were repeated twice with similar results (*SI Appendix*, Fig. S4*B*). (*D*) LST-1 stained for isoform-specific epitope-tags (15): Top, FLAG antibodies detect LST-1L (yellow); bottom, V5 antibodies detect LST-1S (yellow). (*Top* and *Bottom*), LMN-1 antibodies detect LAMIN-1 to highlight the inner nuclear envelope (magenta); DAPI shows DNA (cyan). Left images, low magnification. Representative deconvolved single confocal *z*-slices from the *Middle* plane of the distal region of an extruded gonad. White box, GSC nucleus magnified in the *Middle* panel; green box, more proximal (prox) nucleus magnified in the *Right* panel. Middle and left images, higher magnification of boxed regions in the *Left* panel. Arrows mark nuclear LST-1L (*Top*) and LST-1S (*Bottom*). (*E*) Effects of LST-1 variants on LAG-1 abundance. LAG-1^{FLAG} was scored in extruded gonads stained with α-FLAG antibodies, and quantitated with Image J. Each data line represents mean values of α-FLAG signal with background from a no-tag control subtracted; shading shows the SEM. Gonad numbers: *lst-1(+)*, n = 10; *lst-1(ø)*, n = 15; *lst-1(ZnF)*, n = 15; *lst-1(PIM),* n = 15; no-tag control, n = 10. One-way ANOVA with Tukey's post hoc test shows significant differences between *lst-1(+)* and *lst-1(ZnF)* (*P-value* < 0.01), between *lst-1(+)* and *lst-1(ø)* (*P-value* < 0.01), but no significant difference between *lst-1 (+)* vs *lst-1(PIM)* (*P-value* = 0.6) and between *lst-1(ø) and lst-1(ZnF)* (*P-value = 0.8*). (*F*) Effects of LST-1 variants on nuclear NICD abundance. Nuclear NICD abundance was determined using fluorescent ligand HALOTAG® TMR, which binds to Halo-tag fused to NICD. Abundance was graphed as a function of position in the progenitor zone in germ cell diameter and converted to distance in μm from the distal end by a conversion factor of 4.4 gcd/μm. Each data point (circle) shows the mean value for nuclei in that cell row; vertical lines show SEM Gonad numbers: *lst-1(+)*, n = 15; *lst-1(ø)*, n = 18; *lst-1(ZnF)*, n = 20; *lst-1(PIM),* n = 20; no-tag control, n = 15. One-way ANOVA with Tukey's post hoc test shows significant differences between *lst-1(+)* and *lst-1(ZnF)* (*P-value* < 0.01), between *lst-1(+)* and *lst-1(ø)* (*P-value* < 0.01), but no significant difference between *lst-1(+)* vs *lst-1(PIM)* (*P-value* = 0.9) and between *lst-1 (ø) and lst-1(ZnF)* (*P-value = 0.6*).

conclude that wild-type LST-1 lowers NICD abundance in the nucleus and that its Zinc finger is critical for this effect.

LST-1 Zn Finger Mutant Protein Retains Posttranscriptional Activity. We considered the idea that LST-1 is a bipartite regulator, with an N-terminal region dedicated to RNA repression and a C-terminal region dedicated to feedback on Notch-dependent transcription. We had already demonstrated that the C-terminal Zn finger is required to lower Notch-dependent transcription (Fig. 4), but the possibility of a Zinc finger role in RNA repression had not been tested. We therefore asked whether LST-1(ZnF) mutant protein retains the ability to repress RNAs in a tethering assay. To this end, we used the λN22-BoxB system to test LST-1(ZnF) for repression of a reporter RNA when tethered, as done previously for LST-1 and LST-1(PIM) (16). The first steps were to introduce λN22 at the N terminus of an endogenous *lst-1* gene carrying both the Zn finger mutations and a C-terminal V5 tag and to confirm that LST-1(ZnF)$^{V5\text{-}\lambda N22}$ mutant protein was functional (*SI Appendix*, Fig. S5*A*). Reporter strains were then made with LST-1(ZnF)$^{V5\text{-}\lambda N22}$ or LST-1(ZnF)^{V5}, plus a reporter transgene driving expression of a GFP-Histone RNA with three BoxB sites in its 3'UTR. GFP intensities were measured in the distal gonad, as described (16). We found that tethered LST-1(ZnF)$^{V5\text{-}\lambda N22}$ mutant protein could repress expression of the GFP reporter, but untethered LST-1(ZnF)^{V5} mutant protein could not (Fig. 6*A* and *SI Appendix*, Fig. S5*B*). Therefore, LST-1 can repress RNA without its Zn finger.

Discussion

This work reports that LST-1 down-regulates Notch-dependent transcription in addition to its previously known role as a post-transcriptional regulator of mRNA expression (15–17). Several lines of evidence support this conclusion. First, LST-1 is present in the nucleus and lowers production of nascent transcripts from the Notch-dependent *lst-1* and *sygl-1* loci, but not from a Notch-independent locus. Second, an LST-1 Zinc finger mutant increases Notch signaling strength of Notch receptor mutants. Third, LST-1 lowers abundance of two key components of the Notch transcriptional activation complex, the LAG-1 DNA-binding protein and nuclear NICD. Finally, LST-1 coIPs with LAG-1, a key factor in the Notch transcription complex. LST-1 thus feeds back on Notch signaling to dampen its strength and appears to do so directly.

The two LST-1 mechanisms, posttranscriptional and transcriptional, employ distinct parts of the protein and have distinct roles in stem cell regulation (Fig. 6 *B* and *C*). The LST-1 N-terminal region represses RNA targets, an activity that promotes self-renewal and maintains GSCs (15, 16). By contrast, the LST-1 C-terminal region dampens Notch-dependent transcription, a feedback that limits self-renewal and restricts size of the GSC pool (ref. 15, this work). Region-specific motifs are critical to each function: PUF-interacting motifs (PIMs) are required for RNA repression, and a Zinc finger is required for negative feedback on Notch-dependent transcription. Therefore, the LST-1 bifunctionality reflects its bipartite architecture (Fig. 6*C*). However, the two LST-1 isoforms also contribute to this

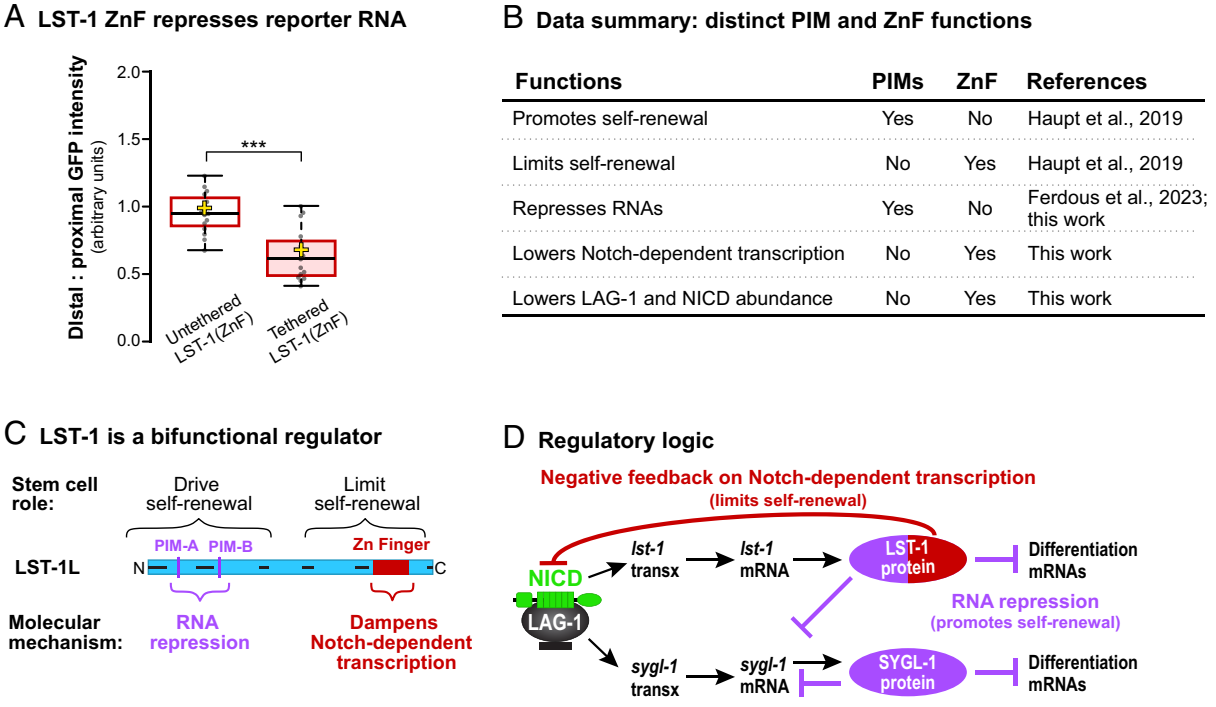

Fig. 6. LST-1 has two central roles in the stem cell regulatory network. (*A*) Tethered LST-1(ZnF)$^{V5\text{-}\lambda N22}$ protein represses expression of a reporter RNA. Tethering assay as described (16), but modified to test LST-1(ZnF)^{V5} protein. Briefly, LST-1(ZnF)^{V5} and LST-1(ZnF)$^{V5\text{-}\lambda N22}$ were introduced into a strain making reporter GFP RNA with "Box B" hairpins in its 3'UTR for recruitment of λN22 peptide. Effects on GFP expression were assayed in the distal germline, (1 to 40 μm from the distal end), where LST-1 is expressed at a high level, and in the more proximal germline (80 to 120 μm from the distal end), where LST-1 is expressed at a vanishingly low level. Shown are boxplots of distal: proximal GFP intensities with untethered LST-1(ZnF)^{V5} (*Left*) or tethered LST-1(ZnF) $^{V5\,\lambda N22}$ (*Right*) with boxplot conventions as described in Fig. 3. Asterisks indicate statistically significant differences (pair-wised Student's *t*.Test). Difference between LST-1(ZnF)^{V5} and LST-1(ZnF)$^{V5\,\lambda N22}$ *P-value* is < 0.0001. Sample sizes: LST-1(ZnF)^{V5}, n = 16; LST-1(ZnF)$^{V5\,\lambda N22}$, n = 16. (*B*) Evidence for distinct LST-1 PIM and ZnF functions. (*C*) Model: LST-1 bifunctionality is based on its bipartite architecture. The LST-1 N-terminal region is sufficient to drive self-renewal because its PIMs are essential for RNA repression (15, 16). The LST-1 C-terminal region limits self-renewal because its Nanos-related Zn finger is essential for negative feedback of Notch-dependent transcription. (*D*) Model: Regulatory logic of GSC stem cell network. The Notch transcription complex activates transcription of *lst-1* and *sygl-1* genes (positive regulation, black arrows to "transx"). The LST-1 and SYGL-1 proteins repress both *sygl-1* and differentiation RNAs (negative regulation, purple lines with barred end) and thereby drive stem cell self-renewal. In addition, LST-1 feeds back on Notch transcription complex, down-regulates its components, and lowers *lst-1* and *sygl-1* transcription (negative regulation, red line with barred end), which lowers LST-1 and SYGL-1 abundance, limits self-renewal, and facilitates differentiation.

bifunctionality. The longer LST-1L isoform possesses both functions (15, 16), but the shorter LST-1S isoform is specialized for Notch feedback (this work). LST-1S lacks PIMs but possesses the Zinc finger and this isoform is sufficient to dampen Notch-dependent transcription. Coupling the two LST-1 functions in the single LST-1L protein likely benefits from its intense concentration in the distal-most germ cells, where Notch signaling strength is at its peak and GSCs must be maintained. The presence of LST-1S in this same region bolsters the LST-1L feedback activity, but LST-1S also extends a bit more proximally than LST-1L (15), which likely reinforces the fate switch to differentiation once GSCs have left the niche.

How does LST-1 down-regulate Notch-dependent transcription? LST-1 physically interacts with LAG-1, and lowers the levels of LAG-1 and NICD, both key components of the Notch activation complex. LST-1 activity therefore likely leads to destabilization of the CSL-NICD complex. We do not yet know the molecular mechanism responsible for this regulation, but its reliance on the LST-1 Zinc finger provides a clue. Some Zn finger proteins bind ubiquitin to promote protein degradation (25–27), so LST-1 may similarly recruit ubiquitin to the Notch transcription complex. Other Zn fingers affect nuclear import (28, 29), so another possibility is that LST-1 inhibits nuclear import of Notch complex components. By yeast two-hybrid, LST-1 binds IMB-2, the *C. elegans* importin β2 homolog so a mechanism involving nuclear import is plausible (30). Regardless of biochemical specifics, LST-1 clearly dampens Notch-dependent transcription and joins a variety of factors that modulate the Notch activation complex (31).

The LST-1 negative feedback on GLP-1/Notch signaling strength introduces a major feature in the regulatory network specialized for balancing self-renewal and differentiation in the *C. elegans* germline (Fig. 6*D*). This feedback must facilitate GSC exit from a stem cell state to differentiation because its loss expands the GSC pool (15). However, LST-1 feedback does not act alone. The *gld-1* RNA is a target of LST-1 and SYGL-1 RNA repression in the distal germline (17), and the GLD-1 RNA-binding protein, which is made upon release from repression in GSCs, can bind *glp-1/Notch* RNA and lower receptor expression (32). In addition, the FBF-2 RNA-binding protein binds to *glp-1/Notch* and *lag-1* RNAs and likely represses them in GSCs. GLD-1 and FBF-2 thus join LST-1 in negatively regulating Notch to promote differentiation of germline stem cells. However, because GLD-1 and FBF-2 are not Notch targets and their abundance is relatively low in the distal-most GSCs, their Notch regulation is likely delayed. By contrast, the *lst-1* gene is a direct target of Notch signaling and LST-1 protein is highly concentrated in the distal-most GSCs. LST-1 therefore likely provides the most immediate feedback.

The Notch signaling pathway regulates stem cells and cell fates broadly among metazoans, and as in *C. elegans,* Notch signaling strength is tightly regulated to orchestrate developmental events in time and space (31). Although LST-1 is a novel protein, its activities have intriguing parallels to fly and mammalian regulators. First and arguably most similar to LST-1, Drosophila Brat and its human homolog TRIM3 protein are bifunctional: They associate with PUF proteins and repress RNAs (33), and they also down-regulate Notch. Indeed, Brat/TRIM3 down-regulates Notch by binding to importin β2 and inhibiting NICD transport into the nucleus (34), a mechanism that LST-1 may also use (described above). The regulatory logic of coupling PUF-mediated RNA repression with Notch negative feedback is thus retained from worms to humans, even though the proteins are different and detailed mechanisms cannot yet be compared. Second, the NOTCH regulated ankyrin repeat protein (NRARP) gene is a direct Notch target (35), and its protein physically interacts with both CSL (mammalian LAG-1) and NICD proteins and inhibits Notch signaling (36–38). Moreover, NRARP overexpression lowers NICD abundance by promoting degradation. An important direction for the future is understanding whether LST-1 down-regulates Notch by inhibiting nuclear import of the NICD, like Brat/TRIM3, promoting protein instability like NRARP or some other mechanism.

Materials and Methods

Nematode Strain Maintenance. Most nematode strains were maintained at 20 °C using standard culture methods (39). *glp-1* temperature-sensitive strains (*ar202* and *q231*) were maintained at 15 °C and shifted to 20 °C and 25 °C for experimentation. For a full list of strains used in this study, see *SI Appendix*, Table S1.

CRISPR-Cas9 Genome Engineering. CRISPR-Cas9 genome editing methods were used with a coconversion strategy to alter endogenous *lst-1* and *lag-1* alleles using ribonuclease complexes following previously described protocols (40, 41). For detailed protocol, see ref. 15. 3xFLAG-tag was inserted at the C terminus in the endogenous *lag-1* gene, the same site where a 3xHA epitope-tag had been inserted before (42). Briefly, progeny of injected hermaphrodites were visually screened for coinjection marker editing and then screened by PCR and Sanger sequencing to confirm the edit. Sequences of all crRNA and DNA templates (both from IDT) are listed in *SI Appendix*, Table S2.

Staining, Microscopy, and Fluorescence Quantitation. Immunostaining of dissected gonads was done as described previously (15, 43). Animals were staged to 24 h past mid-L4 stage before dissection. Primary antibodies were added at following dilutions: mouse α-FLAG (1:1,000, M2 clone, #F3165Sigma), mouse α-V5 (SV5-Pk1, 1:1,000, MCA1360, Bio-Rad), and α-LMN-1 (1:500, #3853002, Novus Biologicals). Secondary antibodies were added in following dilutions: Donkey Alexa 647 α-mouse (1:500, Invitrogen #A31571). For nuclear staining of GLP-1 with halo-tag (HaloTag® TMR Ligand, Promega, #G8252), we followed a previous protocol (24) with minor modification: ligand was added in 1:1,000 dilution after gonad dissection and then incubated 30 min. For both types of staining, DAPI was added at 1 ng/μL final concentration to visualize DNA. Samples were mounted in ProLong Gold and cured overnight in dark before imaging. Images were taken using a laser scanning Leica TCS SP8 confocal microscope with LASX software. Photomultiplier (PMT) detectors were used for DAPI and Hybrid (HyD) detectors for all other flours. A 63×/1.40 CS2 HC Plan Apochromat oil immersion objective was used for all images, which were taken with the standard 400-700Â Hz scanning speed and zoom 100 to 300%. Immunostaining quantitation for cytoplasmic proteins was performed using Fiji/ImageJ following previously described protocols (15). Confocal images in Figs. 2 and 5*D* were processed using the Leica Lightning deconvolution package; images of GSCs and proximal nuclei were processed identically.

Quantitation of nuclear proteins was done using a single z-slice that had the distal tip cell visible to mark the distal end. We used the oval area selection tool and ROI manager to create a standard ROI in FIJI and select DAPI-stained nuclei. Protein abundance (pixel count) was measured in the appropriate channel in multiple nuclei in the same z-slice. Average nuclear protein abundance was plotted against position along the progenitor zone axis in number of cell rows (gcd). Cell rows were also converted to microns using a conversion factor of 4.4 μm/gcd.

smFISH and MATLAB Detection. Worms were staged to 24 h past mid-L4 stage and gonads dissected and prepared for smFISH as described in previous works (14, 18). All smFISH probes used in this study are listed in *SI Appendix*, Table S3. Final concentration of both *lst-1* intron and exon specific probe sets was 0.5 μM. Final concentrations of *sygl-1* intron and exon probe sets were 0.5 μM and 0.25 μM, respectively. Final concentration for *let-858* probe set was 0.5 μM. The MATLAB codes used for smFISH image analysis in this work were previously described (14, 18, 20).

Imaris Detection of *lst-1* ATS. Imaris software (version 9.9.0) was used to detect *lst-1* ATS. We validated this approach by comparing *sygl-1* datasets with MATLAB and Imaris (*SI Appendix*, Fig. S2). The Imaris spot detection algorithm was used to detect intron and exon spots. Model PSF-elongation was used to detect spots,

with the estimated z diameter set as default (2× pixel size). The same contrast settings were used for all germlines analyzed. For the intron channel, a sum intensity filter was applied, and for the exon channel, a mean intensity filter was applied. ATS were defined as exon and intron spots whose centers were no more than 0.2 μm apart and that overlapped with DAPI.

Reporter Tethering assay and GFP Quantitation. Tethering assay quantitation was performed as described (16). Briefly, GFP intensity was measured using FIJI at one distal region and one proximal region within the progenitor zone, and the ratio of GFP intensities in the distal and proximal regions was calculated in Microsoft Excel. Samples from two independent replicates for each genotype were analyzed, and background was normalized to a wild-type control that had no GFP. Sample sizes are reported in the Fig. 4 legend.

Co-Immunoprecipitation and Western Blot Analysis. Co-IPs and western blot analyses were done as described (16). *glp-1 (ts gf)* mutants were synchronized and grown at 25 °C, and extracts were collected from these worms. Mouse α-FLAG (M2 clone, Sigma #F3165) was used to immunoprecipitate LAG-1^{FLAG} and to see LAG-1^{FLAG} on western blots. Mouse α-V5 (Bio-Rad #MCA1360) was used to detect co-immunoprecipitated LST-1^{V5} on western blots. Mouse α-actin (1:40,000, C4 clone, Millipore #MAB1501) was used to detect the actin loading control. For secondary antibodies, blots were incubated for 1 h at RT with Rat HRP-conjugated α-mouse (1:10,000, Abcam mAb 131368). To analyze the co-immunoprecipitations, blots were stripped with Restore™ Western Blot Stripping Buffer (Thermo Scientific). Immunoblots were developed using SuperSignal™West Pico/Femto Sensitivity substrate (Thermo Scientific #34080, #34095) and imaged using an ImageQuant LAS4000 (GE Healthcare). Image contrast was adjusted with FIJI/Image J. Co-IPs were done at least twice for each experiment.

Glp Sterility. Glp sterility is typical of *glp-1* loss-of-function mutants, which lose GSCs and make no embryos (12). To score Glp sterility, N2 wild-type, JK509, JK6011, and JK6725 strains were raised at permissive temperature (15 °C). Adults were bleach synchronized and L1s shifted to restrictive temperature (25 °C). At 24 h past mid-L4 stage, worms were mounted to observe germline size and the presence of embryos under the Nomarski interference contrast microscope (Zeiss Axioimager microscope). Glp sterile animals had smaller than normal germlines and did not make embryos. Suppression of Glp sterility produces embryos, which were scored to confirm Glp embryonic lethality (44).

Statistical Analysis. Statistical analyses, sample sizes, and *P* values are described in figure legends. A two-tailed Student's *t*.test (T.TEST function in Microsoft Excel) assuming equal-variance was done when comparing two samples. A *P* value less than 0.01 was considered significant. Box plots were generated with web tool BoxPlotR (45), and quartiles and whiskers are indicated in legends. For more than two samples, one-way ANOVA and Tukey's post hoc tests were performed to calculate statistical significance using R with a *P* value cutoff set at 0.01. For the line graphs in Figs. 1 and 5, statistical comparisons were done using the highest values obtained for each of the multiple germlines assayed for each variant.

Data, Materials, and Software Availability. Protocols and smFISH codes (MATLAB) are referenced as appropriate throughout the paper. All other data are published with the paper. All study data are included in the article and/or *SI Appendix*.

ACKNOWLEDGMENTS. We thank members of the Kimble lab for helpful discussions throughout the course of this work; Peggy Kroll-Conner for assistance with strain building; and Laura Vanderploeg for help with figures. A.S.F. was supported by a Kamaluddin Ahmad Distinguished Graduate Scholarship; T.R.L. was supported by a NSF Graduate Research Fellowship, Grant No. DGE-1747503; J.K. was supported by NIH R01 GM134119. Any opinions, findings, and conclusions or recommendations expressed in this material are those of the authors and do not necessarily reflect the views of the NSF.

Author affiliations: [a]Department of Biochemistry, University of Wisconsin-Madison, Madison, WI 53706; and [b]Integrated Program in Biochemistry, University of Wisconsin-Madison, Madison, WI 53706

1. L. Li, T. Xie, Stem cell niche: Structure and function. *Annu. Rev. Cell Dev. Biol.* **21**, 605–631 (2005).
2. C. R. Walkley *et al.*, A microenvironment-induced myeloproliferative syndrome caused by retinoic acid receptor **γ** deficiency. *Cell* **129**, 1097–1110 (2007).
3. S. W. Lane *et al.*, The Apcmin mouse has altered hematopoietic stem cell function and provides a model for MPD/MDS. *Blood, J. Am. Soc. Hematol.* **115**, 3489–3497 (2010).
4. A. D. Lander *et al.*, What does the concept of the stem cell niche really mean today? *BMC Biol.* **10**, 1–15 (2012).
5. G. M. Crane, E. Jeffery, S. J. Morrison, Adult haematopoietic stem cell niches. *Nat. Rev. Immunol.* **17**, 573–590 (2017).
6. C. A. Chacón-Martínez, J. Koester, S. A. Wickström, Signaling in the stem cell niche: Regulating cell fate, function and plasticity. *Development* **145**, dev165399 (2018).
7. J. P. Andreotti *et al.*, Neural stem cell niche heterogeneity. *Semin. Cell Dev. Biol.* **95**, 42–53 (2019).
8. A. Kershner *et al.*, Germline stem cells and their regulation in the nematode Caenorhabditis elegans. *Adv. Exp. Med. Biol.* **786**, 29–46 (2013).
9. E. J. Albert Hubbard, T. Schedl, Biology of the Caenorhabditis elegans germline stem cell system. *Genetics* **213**, 1145–1188 (2019).
10. J. Kimble, J. White, On the control of germ cell development in Caenorhabditis elegans. *Dev. Biol.* **81**, 208–219 (1981).
11. A. M. Kershner, H. Shin, T. J. Hansen, J. Kimble, Discovery of two GLP-1/Notch target genes that account for the role of GLP-1/Notch signaling in stem cell maintenance. *Proc. Natl. Acad. Sci. U.S.A.* **111**, 3739–3744 (2014).
12. J. Austin, J. Kimble, glp-1 is required in the germ line for regulation of the decision between mitosis and meiosis in C. elegans. *Cell* **51**, 589–599 (1987).
13. J. L. Brenner, T. Schedl, Germline stem cell differentiation entails regional control of cell fate regulator GLD-1 in Caenorhabditis elegans. *Genetics* **202**, 1085–1103 (2016).
14. C. Lee, E. B. Sorensen, T. R. Lynch, J. Kimble, C. elegans GLP-1/Notch activates transcription in a probability gradient across the germline stem cell pool. *Elife* **5**, e18370 (2016).
15. K. A. Haupt *et al.*, The molecular basis of LST-1 self-renewal activity and its control of stem cell pool size. *Development* **146**, dev181644 (2019).
16. A. S. Ferdous *et al.*, The in vivo functional significance of PUF hub partnerships in C. Elegans germline stem cells. *Development* **150**, dev201705 (2023).
17. H. Shin *et al.*, SYGL-1 and LST-1 link niche signaling to PUF RNA repression for stem cell maintenance in Caenorhabditis elegans. *PLoS Genet.* **13**, e1007121 (2017).
18. T. R. Lynch, M. Xue, C. W. Czerniak, C. Lee, J. Kimble, Notch-dependent DNA cis-regulatory elements and their dose-dependent control of C. Elegans stem cell self-renewal. *Development* **149**, dev200332 (2022).
19. J. Reboul *et al.*, C. elegans ORFeome version 1.1: Experimental verification of the genome annotation and resource for proteome-scale protein expression. *Nat. Genet.* **34**, 35–41 (2003).
20. S. L. Crittenden *et al.*, Sexual dimorphism of niche architecture and regulation of the Caenorhabditis elegans germline stem cell pool. *Mol. Biol. Cell* **30**, 1757–1769 (2019).
21. I. Greenwald, R. Kovall, Notch signaling: Genetics and structure. *WormBook* **17**, 1–28 (2018).
22. S. Christensen, V. Kodoyianni, M. Bosenberg, L. Friedman, J. Kimble, lag-1, a gene required for lin-12 and glp-1 signaling in Caenorhabditis elegans, is homologous to human CBF1 and Drosophila Su (H). *Development* **122**, 1373–1383 (1996).
23. A. S. Pepper, D. J. Killian, E. J. A. Hubbard, Genetic analysis of Caenorhabditis elegans glp-1 mutants suggests receptor interaction or competition. *Genetics* **163**, 115–132 (2003).
24. E. B. Sorensen, H. S. Seidel, S. L. Crittenden, J. H. Ballard, J. Kimble, A toolkit of tagged glp-1 alleles reveals strong glp-1 expression in the germline, embryo, and spermatheca. *Micropublication Biol.* **22**, 2020 (2020).
25. I. Dikic, S. Wakatsuki, K. J. Walters, Ubiquitin-binding domains–from structures to functions. *Nat. Rev. Mol. Cell Biol.* **10**, 659–671 (2009).
26. L. Hicke, H. L. Schubert, C. P. Hill, Ubiquitin-binding domains. *Nat. Rev. Mol. cell Biol.* **6**, 610–621 (2005).
27. J. H. Hurley, S. Lee, G. Prag, Ubiquitin-binding domains. *Biochem. J.* **399**, 361–372 (2006).
28. K. J. Quadrini, J. J. Bieker, Krüppel-like zinc fingers bind to nuclear import proteins and are required for efficient nuclear localization of erythroid Krüppel-like factor. *J. Biol. Chem.* **277**, 32243–32252 (2002).
29. M. Hatayama *et al.*, Functional and structural basis of the nuclear localization signal in the ZIC3 zinc finger domain. *Hum. Mol. Genet.* **17**, 3459–3473 (2008).
30. A. J. Walhout *et al.*, Protein interaction mapping in C. Elegans using proteins involved in vulval development. *Science* **287**, 116–122 (2000).
31. S. J. Bray, Notch signalling in context. *Nat. Rev. Mol. Cell Biol.* **17**, 722–735 (2016).
32. B. M. Farley, S. P. Ryder, POS-1 and GLD-1 repress glp-1 translation through a conserved binding-site cluster. *Mol. Biol. Cell* **23**, 4473–4483 (2012).
33. T. A. Edwards, B. D. Wilkinson, R. P. Wharton, A. K. Aggarwal, Model of the brain tumor–Pumilio translation repressor complex. *Genes Dev.* **17**, 2508–2513 (2003).
34. S. Mukherjee *et al.*, Drosophila Brat and human ortholog TRIM3 maintain stem cell equilibrium and suppress brain tumorigenesis by attenuating Notch nuclear transport. *Cancer Res.* **76**, 2443–2452 (2016).
35. L. T. Krebs, M. L. Deftos, M. J. Bevan, T. Gridley, The Nrarp gene encodes an ankyrin-repeat protein that is transcriptionally regulated by the notch signaling pathway. *Dev. Biol.* **238**, 110–119 (2001).
36. E. Lamar *et al.*, Nrarp is a novel intracellular component of the Notch signaling pathway. *Genes Dev.* **15**, 1885–1899 (2001).
37. S. M. Jarrett *et al.*, Extension of the Notch intracellular domain ankyrin repeat stack by NRARP promotes feedback inhibition of Notch signaling. *Sci. Signal.* **12**, eaay2369 (2019).
38. T. J. Yun, M. J. Bevan, Notch-regulated ankyrin-repeat protein inhibits Notch1 signaling: Multiple Notch1 signaling pathways involved in T cell development. *J. Immunol.* **170**, 5834–5841 (2003).
39. S. Brenner, The genetics of Caenorhabditis elegans. *Genetics* **77**, 71–94 (1974).

40. J. A. Arribere *et al.*, Efficient marker-free recovery of custom genetic modifications with CRISPR/Cas9 in Caenorhabditis elegans. *Genetics* **198**, 837–846 (2014).
41. A. Paix, A. Folkmann, D. Rasoloson, G. Seydoux, High efficiency, homology-directed genome editing in Caenorhabditis elegans using CRISPR-Cas9 ribonucleoprotein complexes. *Genetics* **201**, 47–54 (2015).
42. J. Chen *et al.*, GLP-1 Notch–LAG-1 CSL control of the germline stem cell fate is mediated by transcriptional targets lst-1 and sygl-1. *PLoS Genet.* **16**, e1008650 (2020).
43. S. L. Crittenden, H. S. Seidel, J. Kimble, Analysis of the C. Elegans germline stem cell pool. *Methods Mol. Biol.* **2677**,
44. J. R. Priess, H. Schnabel, R. Schnabel, The glp-1 locus and cellular interactions in early C. Elegans embryos. *Cell* **51**, 601–611 (1987).
45. M. Spitzer, J. Wildenhain, J. Rappsilber, M. Tyers, BoxPlotR: A web tool for generation of box plots. *Nat. Methods* **11**, 121–122 (2014).